Research Square

Preprints are preliminary reports that have not undergone peer review.
They should not be considered conclusive, used to inform clinical practice,
or referenced by the media as validated information.

Novel Hybrid Composite Spindle Shaft for Horizontal Peripheral Milling: A Dynamic Behavior Analysis and Surface Roughness Assessment

Everton Medeiros

everton.medeiros@gp.ita.br

Instituto Tecnologico de Aeronautica https://orcid.org/0000-0001-6912-6726

Mauro Mathias

Manoel Alves

Research Article

Keywords: Peripheral milling, CFRP, Orbit Analysis, Surface Roughness

Posted Date: November 6th, 2026

DOI: https://doi.org/10.21203/rs.3.rs-11448203/v1

License: This work is licensed under a Creative Commons Attribution 4.0 International License.
Read Full License

Novel Hybrid Composite Spindle Shaft for Horizontal Peripheral Milling: A Dynamic Behavior Analysis and Surface Roughness Assessment

Everton Coelho de Medeiros[1*], Mauro Hugo Mathias[2] and Manoel Cleber Silva Alves[2]

[1*]Mechanical Engineering Division, Instituto Tecnológico de Aeronáutica, Praça Marechal Eduardo Gomes, São José dos Campos, 12228-900, São Paulo, Brazil.
[2]Mechanical Engineering Department, Universidade Estadual Paulista "Júlio de Mesquita Filho", Avenida Dr. Ariberto Pereira da Cunha, Guaratinguetá, 12516-410, São Paulo, Brazil.

*Corresponding author(s). E-mail(s): coelhoecm@ita.br;
Contributing authors: mauro.h.mathias@unesp.br;
manoel.alves@unesp.br;

Abstract

Vibration damping in machine tool spindle systems is vital for suppressing dynamic instability during severe intermittent cutting operations. While carbon fiber reinforced polymer (CFRP) composites have been explored for high-speed vertical spindles and external damping attachments, their direct integration within horizontal spindle shafts for conventional tangential milling remains unprecedented. Addressing this gap, this paper introduces a hybrid CFRP horizontal spindle shaft achieving a **55.5%** reduction in rotating mass and an exceptionally high damping ratio of **14.58%** and delivers a comprehensive real-world experimental assessment of its dynamic response and workpiece surface finish. The findings reveal that under high-speed cutting regimes (**1560** rpm), the hybrid shaft acts as a passive structural filter, suppressing high-frequency resonant peaks (**350**–**450** Hz band) and unlocking significant performance gains essential for high-productivity machining. Under high material removal rates, peak surface topography metrics are substantially enhanced, reducing $\boldsymbol{R_z}$ by up to **27.5%** and $\boldsymbol{R_t}$ by up to **34.2%**. Furthermore, the particular physical conditions governing the process, including low feed-per-tooth regimes, are thoroughly mapped using orthogonal orbital trajectories ($\boldsymbol{R}$), FFT spectra, and surface

topography. These insights demonstrate the viability of hybrid CFRP shafts for boosting productivity in tangential milling while defining clear operational boundaries for industrial adoption.

Keywords: Peripheral milling, CFRP, Orbit Analysis, Surface Roughness

1 Introduction

In modern manufacturing industries, achieving high surface integrity and dimensional accuracy in machining processes is paramount. Peripheral (or horizontal tangential) milling using disc cutters is widely employed for producing keyways, slots, and complex planar profiles. However, the inherent intermittent nature of tangential milling exposes the machine tool system to cyclic impact loads every time a tooth engages the workpiece. These periodic shock forces induce dynamic instability, severe tool-spindle vibrations, and regenerative chatter, which directly degrade surface quality and accelerate tool wear Ozoegwu and Okokpujie (2021); Grechaniuk and Varodov (2025).

To mitigate dynamic excitation and improve surface finish, various damping strategies have been integrated into machine tools. Traditional approaches encompass passive tuned mass dampers (TMDs), active electromagnetic or hydraulic spindle bearings, constrained layer damping applied to toolholders, and impact-damped tools Wan et al. (2019); Ma et al. (2021); Yang et al. (2015). While these external systems have demonstrated effectiveness in suppressing vibration amplitudes and improving surface roughness by up to 20–40% Kim and Ahn (2024), they often introduce operational complexity, increase rotordynamic inertia, or require costly control units. Consequently, incorporating intrinsic structural damping directly into the rotating spindle shaft represents a more elegant, passive, and robust alternative.

Over the past decade, Carbon Fiber Reinforced Polymer (CFRP) composites have emerged as promising materials for primary structural components in precision machine tools due to their high specific stiffness, light weight, and remarkably high internal damping capacity Zheng et al. (2024); Kim et al. (2022); Liu et al. (2016). Existing literature has explored composite materials in high-speed motorized spindles, boring bars, and vertical face grinding setups, mainly highlighting weight reduction, thermal growth suppression, and dynamic stiffness enhancement Li et al. (2026); Kondo et al. (2020); Aggogeri et al. (2017); Birk et al. (2020). However, a significant gap remains in the scientific literature regarding the application of hybrid CFRP composite spindles in horizontal tangential milling setups. Furthermore, existing rotordynamic studies on composite shafts predominantly focus on frequency response functions (FRF) or critical speeds, rarely bridging the gap between non-linear orbital dynamics, harmonic spectra attenuation, and specific surface topography parameters (R_a, R_z, and R_t).

To address this knowledge gap, this study presents a comprehensive experimental investigation into the dynamic response and surface finish characteristics of a horizontal tangential milling process operating with a hybrid CFRP composite spindle shaft.

The dynamic performance of the composite shaft is analyzed via orbital trajectories and Fast Fourier Transform (FFT) frequency spectra ($1X$ and $2X$ harmonics) and directly compared against a conventional steel shaft under identical cutting conditions. The resulting surface integrity is evaluated using arithmetic mean roughness (R_a), maximum height of profile (R_z), and total height of profile (R_t). This work highlights the physical role of the composite shaft's high internal damping as a passive "structural filter" against transient shock forces, providing new insights into the decoupling between kinematic-driven roughness (R_a) and vibration-sensitive peak parameters (R_z/R_t).

2 Experimental Methodology

To investigate the influence of structural damping on rotordynamic behavior and workpiece surface topography, comparative experimental tests were conducted using a conventional steel spindle shaft and a hybrid carbon fiber reinforced polymer (CFRP) composite spindle shaft mounted in a horizontal milling machine.

2.1 Spindle Shaft Architecture and Material Properties

To investigate the dynamic behavior and damping performance during horizontal tangential milling, two spindle shafts with identical overall primary dimensions were evaluated: the original monolithic steel shaft supplied with the milling machine and a custom-built hybrid carbon fiber reinforced polymer (CFRP) composite shaft. While the steel shaft is solid with a nominal diameter of 22 mm, the CFRP shaft features a tubular geometry with an outer diameter of 22 mm and an inner diameter of 18 mm. Both shafts present an overall length of 500 mm. In the milling machine assembly, the shaft is supported between two boundary regions separated by a total span of 500 mm between supports. The drive end, where torque is transmitted, is housed within precision rolling element bearings, whereas the opposite outboard support region rests on a sliding journal bearing.

The tool clamping arrangement is situated at the mid-span of the shaft length to accommodate a disc milling cutter. Axial location and securing of the disc cutter are accomplished using a set of cylindrical spacer rings fitted over the 22 mm diameter shaft. Dynamic locking and tool retention are achieved through friction clamping, driven by tightening a fine-thread left-hand nut (MF 22×1.5) at the threaded end of the shaft assembly, which compresses the spacer rings and cutter against an axial shoulder.

While the reference steel shaft is the solid original equipment manufacturer (OEM) component of the milling machine, the hybrid composite shaft was custom-fabricated by joining a tubular CFRP main body, made of carbon fiber impregnated with epoxy resin, to two machined steel end-fittings required for machine tool integration. At the torque transmission drive end, the hybrid shaft utilizes a steel fitting featuring a standard Morse Taper 2 (MT2) shank with an internal M16 thread designed to engage the machine drawbar. Connection between the CFRP tube and the steel MT2 fitting was achieved using Henkel LOCTITE HY 4090 hybrid adhesive, which was

applied to the external surface of the composite shaft prior to inserting it into a precision-machined internal recess of the steel MT2 shank.

To establish the structural wall architecture of the tubular CFRP body, cross-sectional samples extracted from the shaft were polished and characterized via optical microscopy (Figure 1). Microstructural analysis reveals a hybrid laminate architecture consisting of 10 alternating unidirectional (UD) carbon fiber layers stacked in a $[0°/90°]_5$ sequence from the inner bore toward the outer wall. This alternating orientation provides a balanced trade-off between axial/flexural stiffness (0° longitudinal fibers) and hoop structural integrity against radial compression (90° transversal fibers). As observed in the outermost region, the layup transitions into a plain woven fabric layer exhibiting characteristic fiber crimp (undulations), which serves as a protective outer shell enhancing resistance to localized contact loads, surface abrasion, and environmental handling during spindle assembly.

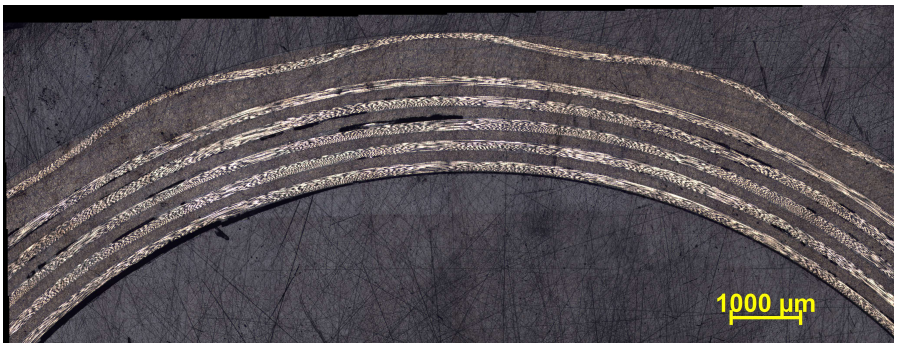


Fig. 1 Cross-sectional optical micrograph of the hybrid CFRP shaft.

At the opposing support end, where the retaining nut provides clamping force, structural bonding was likewise employed using the same adhesive. In this instance, the adhesive was applied to the internal bore of the composite tube to receive a custom-threaded steel insert machined with matching left-hand MF 22×1.5 threads, enabling direct coupling with the milling machine's original locking nut. The bonded joint overlap area and interface dimensions were analytically sized based on the nominal shear strength of the adhesive to ensure that the torsional capacity of the adhesive joint substantially exceeds the maximum operational cutting torque generated during peripheral milling. This prevents torsional slipping and structural debonding under cyclic dynamic excitation. Without the inclusion of the cutting tool, spacer rings, and locking nut, the complete assembly mass of the original steel shaft is 2.38 kg, whereas the custom hybrid CFRP shaft assembly weighs 1.06 kg. This design achieves a 55.5% reduction in total rotating mass, significantly modifying the system's inertia and natural frequency spectrum while enhancing internal passive dissipation via the viscoelastic polymer matrix and bonded joint interfaces (Figure 2 shows both shafts side by side). The geometric, physical, and operational specifications of both shaft configurations are summarized in Table 1.



Fig. 2 CFRP and Steel spindle shaft

Table 1 Physical and mechanical properties of the evaluated spindle shafts

Parameter / Property	Steel Spindle Shaft	Hybrid CFRP Spindle Shaft
Assembly Mass	2.38 kg	1.06 kg
Young's / Flexural Modulus	210 GPa	$E_{\text{eff}} \approx 54.33$ GPa
Measured Damping Ratio**	$\approx 1.5\%$	14.58%

**Experimentally determined via impulse excitation testing using the logarithmic decrement method.

2.2 Setup and Experimental Conditions

Intermittent cutting forces on the composite rotating shaft was simulated through peripheral tangential milling operations on a universal milling machine configured in horizontal spindle mode (Figure 3). A high-speed steel (HSS Type H) disc cutter featuring 12 teeth, an outer diameter of 100 mm, and a width of 10 mm was mounted at the mid-span position of the 22 mm diameter shaft. All machining operations were performed using an up-milling (conventional) cutting direction.

The workpiece specimens consisted of Nylon (Polyamide 6) parallelepiped blocks with dimensions of $40 \times 40 \times 80$ mm, secured within a heavy-duty manual vise. Nylon was deliberately selected for this initial proof-of-concept (PoC) investigation due to its highly homogeneous mechanical behavior, isotropic properties, and low susceptibility to tool wear. This controlled material baseline ensures high experimental repeatability under intermittent tooth engagement while effectively isolating the intrinsic structural damping and passive filtering behavior of the hybrid CFRP shaft from confounding variables such as rapid cutting edge degradation, severe frictional heating, or work-hardening dynamics typical of metallic alloys.

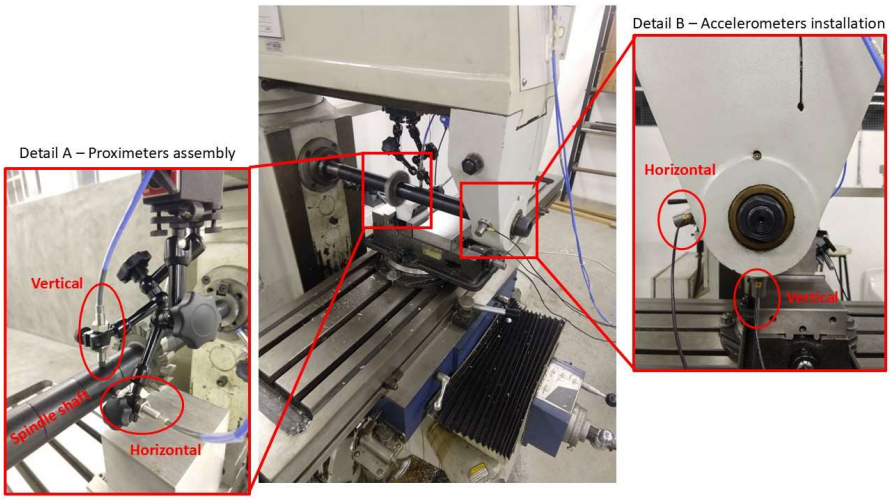


Fig. 3 Experimental horizontal milling set up

The experimental design comprised single-pass cutting trials evaluated across combinations of three spindle speeds (456, 810, and 1560 rpm), two table feed rates (50 and 117 mm/min), and two depths of cut (0.5 and 1.0 mm). For benchmarking and direct dynamic comparison, identical machining conditions were subsequently executed using the original monolithic steel shaft. Real-time dynamic behavior was recorded using a multi-sensor setup applied directly to the machine tool. Shaft flexural deflections and orbital trajectories were captured by two eddy-current proximity probes (2.5 mm linear range) mounted orthogonally at 0° and 90° on the spacer rings immediately adjacent to the cutter. Positioned in close proximity to the cutting zone, these proximeters recorded local shaft displacements resulting from intermittent cutting forces. Detail A from Figure 3 shows the proximeters assembly.

Structural vibration acceleration was monitored using two piezoelectric accelerometers mounted via magnetic bases in the horizontal and vertical directions on the sliding journal bearing housing. The sliding bearing region was selected specifically to isolate cutting-induced dynamic responses from high-frequency electromagnetic and mechanical gear-mesh noise originating from the main drive reduction gearbox. Detail B from Figure 3 shows the accelerometers installation. Real-time rotational speed tracking was simultaneously recorded during cutting using an inductive proximity sensor oriented toward the drive section of the spindle.

Surface quality evaluation was performed post-machining to assess the influence of spindle damping on workpiece topography. Roughness metrics included arithmetic mean roughness (R_a), ten-point height roughness (R_z), and total profile height (R_t), recorded with a standard cut-off wavelength (λ_c) of 2.5 mm across 5 sample evaluation lengths. To ensure statistical consistency, three independent profile sweeps were acquired along the feed path for each specimen, corresponding to the initial, middle, and final regions of the machined surface.

3 Results and Discussion

3.1 Workpiece Surface Quality and Topography

The comparative surface roughness evaluation, detailed in Table 2, demonstrates that the hybrid CFRP shaft performance is strongly dependent on the cutting dynamic regime. By grouping the experimental conditions into high-speed dynamic damping and low-to-moderate speed inertial regimes, clear operational windows emerge for each shaft configuration.

Under high-speed machining conditions ($n = 1560$ rpm), the hybrid CFRP shaft demonstrated superior performance, particularly in mitigating peak-to-valley roughness metrics. For the highest material removal condition ($n = 1560$ rpm, $v_f = 50$ mm/min, $a_p = 1.0$ mm), the hybrid shaft yielded significant improvements over the baseline steel shaft, reducing R_z by 27.5% ($\Delta R_z = +27.5\%$) and R_t by 34.2% ($\Delta R_t = +34.2\%$), with a modest arithmetic roughness gain of $\Delta R_a = +3.5\%$. Similarly, at $n = 1560$ rpm, $v_f = 117$ mm/min, and $a_p = 0.5$ mm, consistent enhancements across all metrics were recorded ($\Delta R_a = +5.0\%$, $\Delta R_z = +20.4\%$, $\Delta R_t = +15.3\%$). These results indicate that under severe dynamic loads and high excitation frequencies, the viscoelastic carbon-fiber matrix effectively absorbs transient force spikes, mitigating tool chatter and suppressing macro-geometric surface defects (R_z, R_t).

A localized performance drop was identified at $n = 1560$ rpm, $v_f = 50$ mm/min, and $a_p = 0.5$ mm, where the hybrid shaft experienced severe surface degradation ($\Delta R_a = -130.5\%$, $\Delta R_z = -173.1\%$, $\Delta R_t = -124.8\%$). This localized anomaly is governed by the interaction between micro-cutting mechanics and structural flexural compliance. At an extremely low feed per tooth ($f_z = 2.67\,\mu$m/tooth), the undeformed chip thickness falls near or below the cutting edge radius of the HSS disc cutter. Under this regime, the dominant cutting mechanism transitions from effective chip shearing to elastic-plastic rubbing and plowing. Plowing drastically alters the cutting force ratio, generating disproportionately high radial thrust forces relative to tangential cutting forces. While the monolithic steel shaft possesses sufficient static flexural rigidity ($E = 210$ GPa) to resist these radial thrust forces without substantial deflection, the lower flexural modulus of the CFRP shaft ($E_{\text{eff}} = 54.33$ GPa) renders it more compliant. The high radial forces induce significant dynamic bending deflections, causing the tool to periodically lift off and re-engage the workpiece surface. This cyclical spring-back effect triggers self-excited horizontal chatter vibrations (evidenced by the dominant spectral bands at 291 Hz, 344 Hz, and 371 Hz in Figure 8), ultimately degrading the surface topography.

In moderate (810 rpm) and low-speed (456 rpm) regimes, the steel shaft consistently yielded superior surface quality across all parameter combinations. At reduced cutting speeds, static cutting forces increase while the viscoelastic damping benefit of CFRP is less effective against static bending deflections. Under these conditions, the higher structural mass and static rigidity of the steel shaft offer superior resistance against static deflections, maintaining tighter surface tolerances during low-speed finishing.

Table 2 Machining performance comparison emphasizing hybrid CFRP shaft gains under high-speed dynamic regimes

Speed n (rpm)	Feed v_f (mm/min)	Depth a_p (mm)	Shaft Configuration	R_a (μm)	R_z (μm)	R_t (μm)	ΔR_a (%)	ΔR_z (%)	ΔR_t (%)
High-Speed / High-Load Regimes (CFRP Damping Window)									
1560	50	1.0	Original Steel	2.30 ± 0.16	13.82 ± 1.94	21.96 ± 2.95	–	–	–
			Hybrid CFRP	2.22 ± 0.27	10.02 ± 1.58	14.45 ± 2.11	**+3.5%**	**+27.5%**	**+34.2%**
1560	117	0.5	Original Steel	1.59 ± 0.06	8.14 ± 1.99	17.32 ± 6.57	–	–	–
			Hybrid CFRP	1.51 ± 0.43	6.48 ± 2.80	14.67 ± 9.69	**+5.0%**	**+20.4%**	**+15.3%**
1560	117	1.0	Original Steel	1.19 ± 0.36	5.15 ± 1.34	8.92 ± 1.47	–	–	–
			Hybrid CFRP	1.40 ± 0.38	5.69 ± 1.47	9.03 ± 2.86	-17.6%	-10.5%	-1.2%
1560	50	0.5	Original Steel	1.79 ± 0.22	8.62 ± 0.85	15.62 ± 2.27	–	–	–
			Hybrid CFRP	4.12 ± 0.79	23.55 ± 6.50	35.11 ± 8.05	-130.2%	-173.2%	-124.8%
Moderate and Low-Speed Regimes (Steel Inertial Stability Window)									
810	117	0.5	Original Steel	0.75 ± 0.10	3.57 ± 0.69	5.76 ± 1.25	–	–	–
			Hybrid CFRP	0.94 ± 0.08	4.38 ± 0.34	6.73 ± 0.75	-25.3%	-22.7%	-16.8%
810	50	0.5	Original Steel	0.97 ± 0.17	3.84 ± 0.36	6.81 ± 2.31	–	–	–
			Hybrid CFRP	1.26 ± 0.10	5.21 ± 0.63	8.12 ± 1.02	-29.9%	-35.7%	-19.2%
456	117	1.0	Original Steel	0.80 ± 0.05	3.49 ± 0.14	5.47 ± 0.48	–	–	–
			Hybrid CFRP	0.92 ± 0.10	4.47 ± 0.59	6.58 ± 0.19	-15.0%	-28.1%	-20.3%
456	117	0.5	Original Steel	0.86 ± 0.07	4.07 ± 0.46	6.52 ± 1.09	–	–	–
			Hybrid CFRP	1.32 ± 0.30	5.37 ± 1.08	8.37 ± 1.41	-53.5%	-31.9%	-28.4%
456	50	1.0	Original Steel	0.67 ± 0.07	2.78 ± 0.55	4.59 ± 1.50	–	–	–
			Hybrid CFRP	1.13 ± 0.29	4.05 ± 1.01	7.08 ± 2.39	-68.7%	-45.7%	-54.2%
456	50	0.5	Original Steel	0.59 ± 0.16	2.75 ± 0.97	3.72 ± 1.01	–	–	–
			Hybrid CFRP	1.20 ± 0.36	4.44 ± 0.80	8.03 ± 2.81	-103.4%	-61.5%	-115.9%

3.2 Shaft Orbital Trajectories and Dynamic Deflections

The dynamic flexural behavior of both spindle shaft configurations was evaluated by analyzing the $X - Y$ orbital trajectories reconstructed from the orthogonal eddy-current displacement sensors positioned near the disc cutter. Figures 4 through 7 display the orbital paths for the CFRP and steel shafts across the four cutting conditions at 1560 rpm. To evaluate the spatial positioning of the shaft under operational loading, each trajectory is characterized by its mean orbit center offset magnitude (R), which represents the net static equilibrium position (DC offset).

Both shaft materials exhibit non-circular, lobed orbit geometries resulting from the superposition of low-order rotational harmonics ($1X$ through $6X$) and the tooth passing frequency ($12X = 312$ Hz). Notably, the CFRP shaft trajectories display more pronounced high-frequency boundary ripples ("lobed" or "hairy" morphology) compared to the smooth paths of the steel shaft. This structural difference stems from the lower mass and density of the composite material, which increases its dynamic response susceptibility to periodic tooth impact forces.

Despite displaying localized boundary ripples due to its reduced rotating mass, the mean center offset magnitude (R) indicates that the CFRP shaft establishes a distinct static equilibrium baseline compared to the baseline steel shaft. Under lower depth-of-cut conditions ($a_p = 0.5$ mm), the steel shaft maintains a static center offset of $R = 15.11$ mm, whereas the CFRP shaft operates at a reduced offset of $R = 14.37 - 14.42$ mm. When the depth of cut is increased to $a_p = 1.0$ mm, the CFRP shaft exhibits a further shift in its mean equilibrium position to $R = 13.10$ mm, while the steel shaft position remains virtually unchanged ($R \approx 15.10 - 15.11$ mm) This systemic reduction in R indicates that, despite displaying localized harmonic ripples on its orbit boundary due to its low mass, the CFRP shaft maintains a tighter overall macro-displacement envelope.

In small depth of cut condition, the lower cutting load results in equivalent macro-orbital envelopes ($R \approx 14.40$ mm^{-1}) and nearly identical orbit center positions for the CFRP shaft. The severe degradation in roughness is observed exclusively when the feed rate is smaller and therefore not driven by global orbital displacement, but by localized micro-cutting instabilities (plowing and rubbing at $f_z = 2.67\,\mu$m/tooth) occurring directly at the tool-workpiece interface.

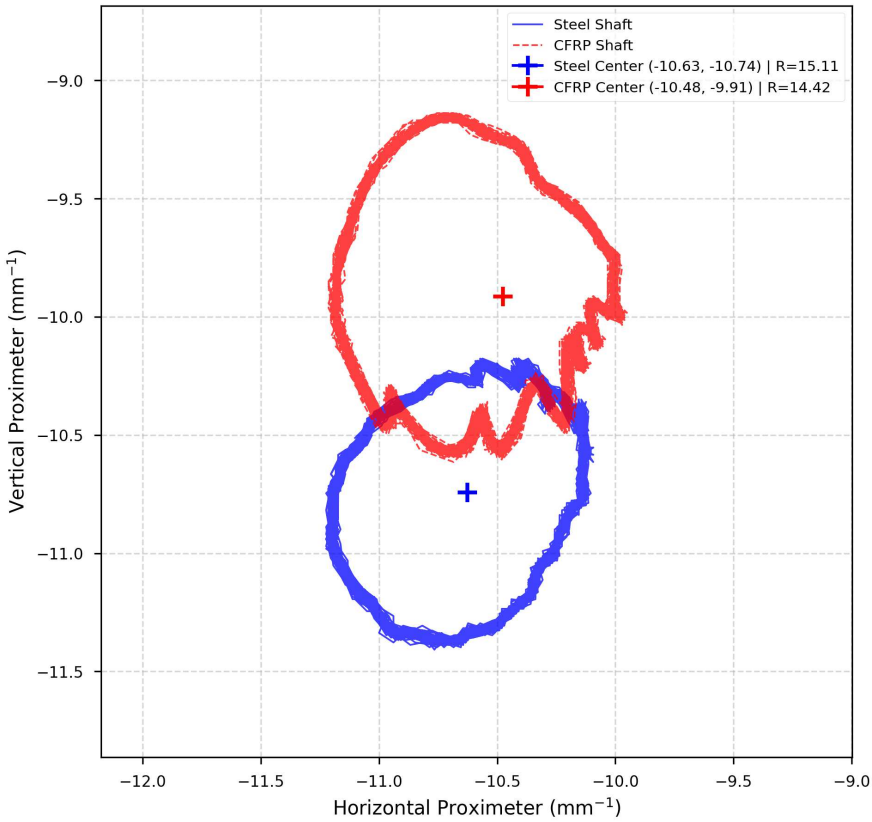


Fig. 4 Shaft orbit plots comparing Steel and CFRP shafts for $n = 1560$ rpm, $v_f = 50$ mm/min, $a_p = 0.5$ mm.

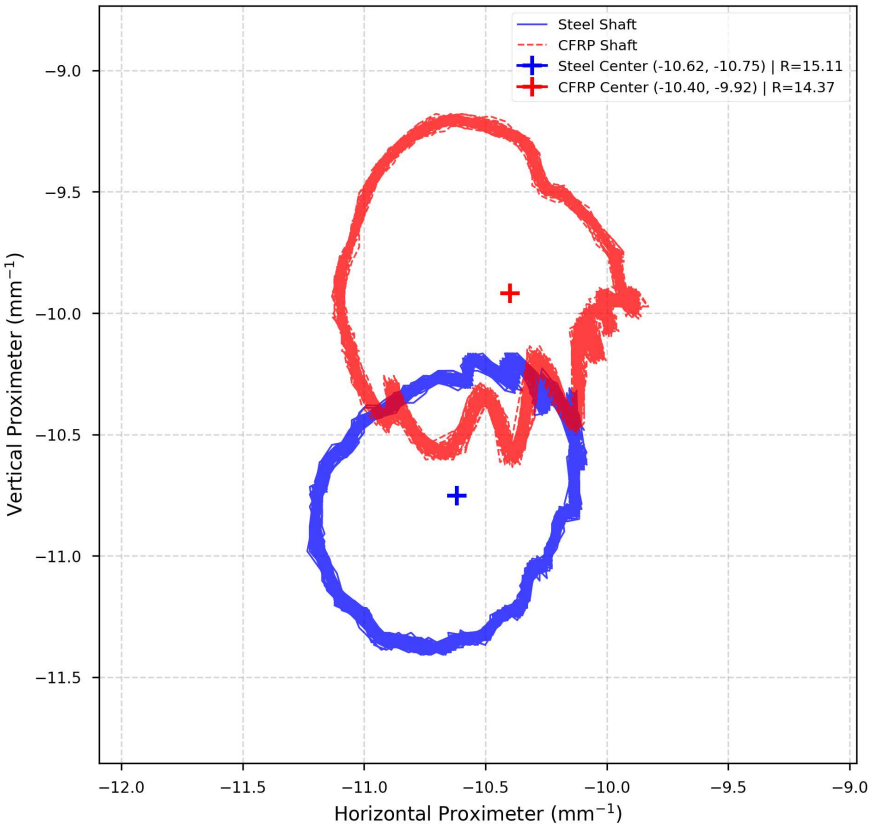


Fig. 5 Shaft orbit plots comparing Steel and CFRP shafts for $n = 1560$ rpm, $v_f = 117$ mm/min, $a_p = 0.5$ mm.

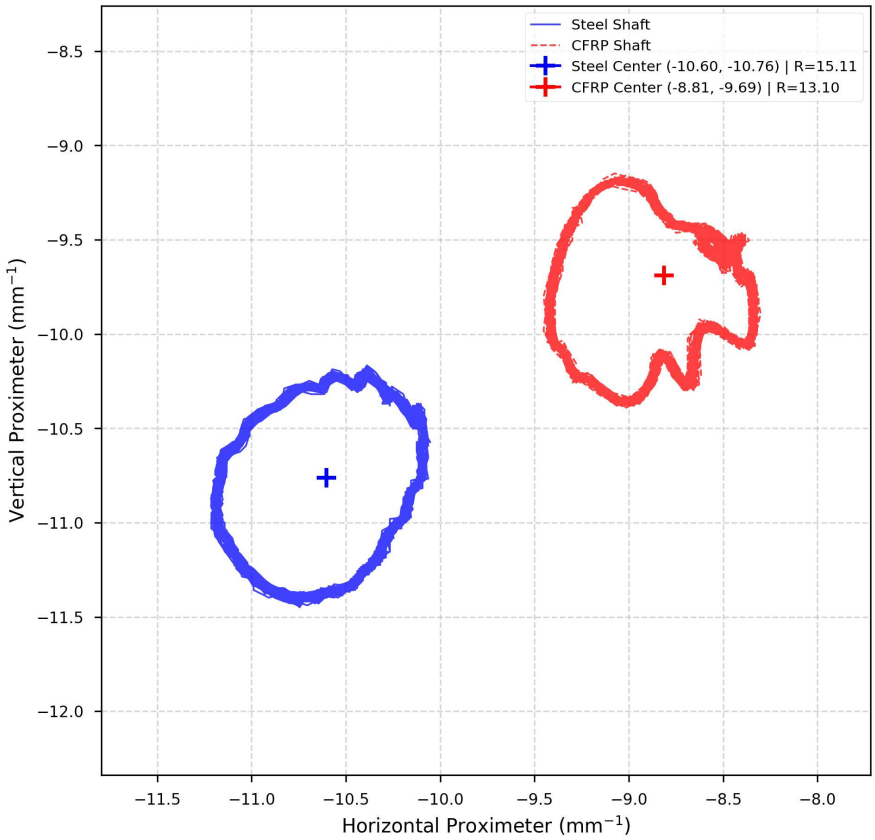


Fig. 6 Shaft orbit plots comparing Steel and CFRP shafts for $n = 1560$ rpm, $v_f = 50$ mm/min, $a_p = 1.0$ mm.

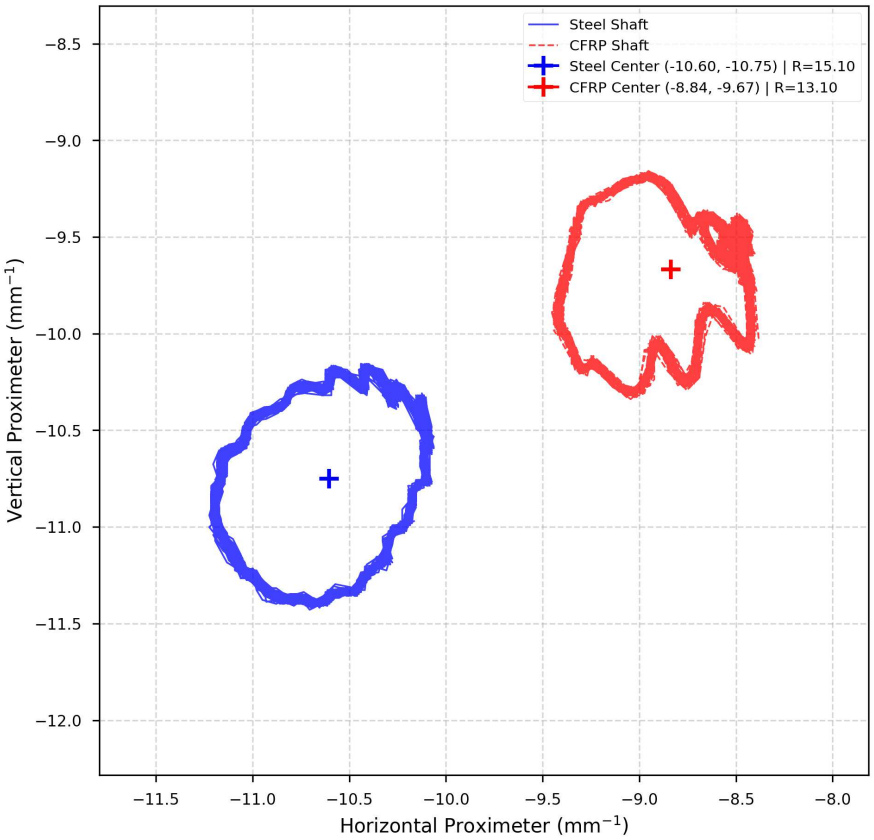


Fig. 7 Shaft orbit plots comparing Steel and CFRP shafts for $n = 1560$ rpm, $v_f = 117$ mm/min, $a_p = 1.0$ mm.

3.3 Spectral Analysis

To understand the physical mechanisms governing the cutting processes and dynamic stability, the frequency spectra obtained from the vertical (*Acc V*) and horizontal (*Acc H*) accelerometers were analyzed for all four operating conditions at 1560 rpm. The shaft rotational frequency is $f_r = 26$ Hz, yielding a tooth passing frequency of $f_{tpf} = 312$ Hz for the 12-tooth cutter.

In the condition test with $v_f = 50$ mm/min and $a_p = 0.5$ mm, the feed per tooth is $f_z = 2.67\,\mu$m/tooth. As a result, the cutting edge predominantly rubs and squeezes the material (plowing/rubbing). The workpiece exerts a spring-back force on the tool, triggering horizontal chatter vibrations. As shown in Figure 8, the horizontal FFT spectrum (*Acc H*) for the CFRP shaft exhibits pronounced high-amplitude vibration bands around the tooth passing frequency, with prominent peaks at 291 Hz (0.95 m/s^2), 344 Hz (1.41 m/s^2) and 371 Hz (1.39 m/s^2). This uncontrolled horizontal vibration energy accounts for the severe degradation in surface generation under this condition.

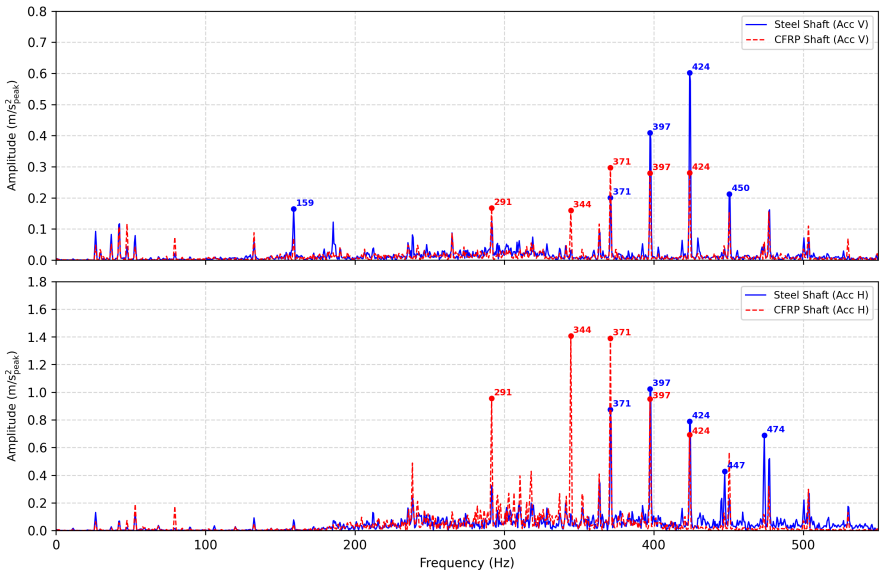


Fig. 8 FFT graph comparing Steel and CFRP shafts for $n = 1560$ rpm, $v_f = 50$ mm/min, $a_p = 0.5$ mm.

In $v_f = 50$ mm/min and $a_p = 1.0$ mm, although the feed per tooth remains low ($f_z = 2.67\,\mu$m/tooth), doubling the depth of cut increases the tool-workpiece contact area and mean cutting forces, mitigating the plowing effect; thus, the high viscoelastic damping capacity of the CFRP polymer matrix becomes the dominant mechanism for dissipating vibrational energy. Figure 9 illustrates the broad suppression of amplitude in the 350 Hz−450 Hz frequency range for the CFRP shaft compared to the steel shaft. While the steel shaft exhibits severe resonant peaks at 398 Hz and 424 Hz (exceeding 1.14 m/s^2), the CFRP shaft maintains horizontal amplitudes below 0.60 m/s^2 and vertical amplitudes below 0.24 m/s^2.

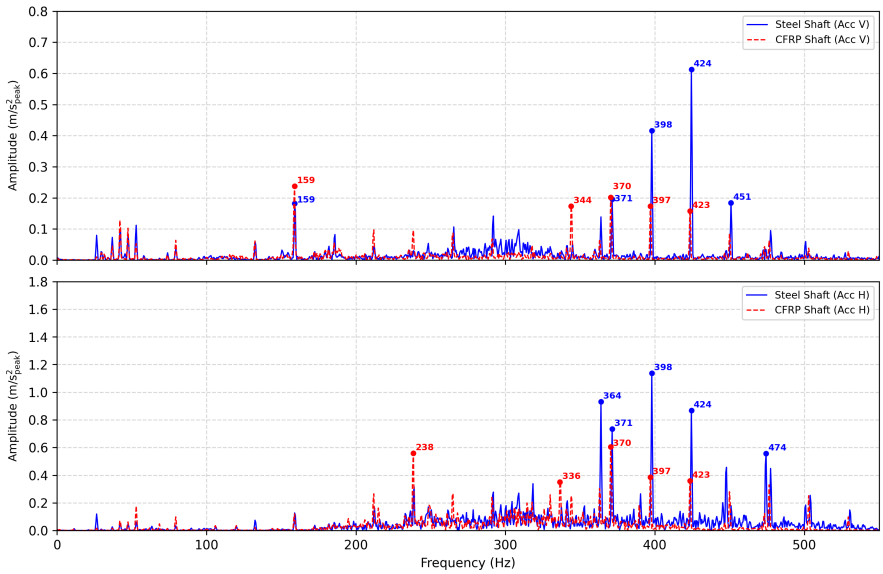


Fig. 9 FFT graph comparing Steel and CFRP shafts for $n = 1560$ rpm, $v_f = 50$ mm/min, $a_p = 1.0$ mm.

In $v_f = 117$ mm/min and $a_p = 0.5$ mm, increasing the feed per tooth to $f_z = 6.25\,\mu$m/tooth elevates the chip thickness. As shown in Figure 10, cutting occurs via effective chip shearing, yielding controlled horizontal vibration peaks at 344 Hz and 371 Hz while suppressing the sharp resonant peaks observed in the steel shaft at 398 Hz and 424 Hz. Conversely, when feed rate and depth of cut are simultaneously maximized in $v_f = 117$ mm/min and $a_p = 1.0$ mm, total cutting forces reach their maximum magnitude. Because CFRP has a lower flexural modulus than steel, the composite shaft experiences increased dynamic bending compliance under heavy loading. As demonstrated in Figure 11, a distinct peak emerges at 238 Hz (0.91 m/s^2 in *Acc H*) exclusively for the CFRP shaft, corresponding to the excitation of its fundamental flexural bending mode. This compliance under high loading alters tool engagement trajectories, reducing process stability.

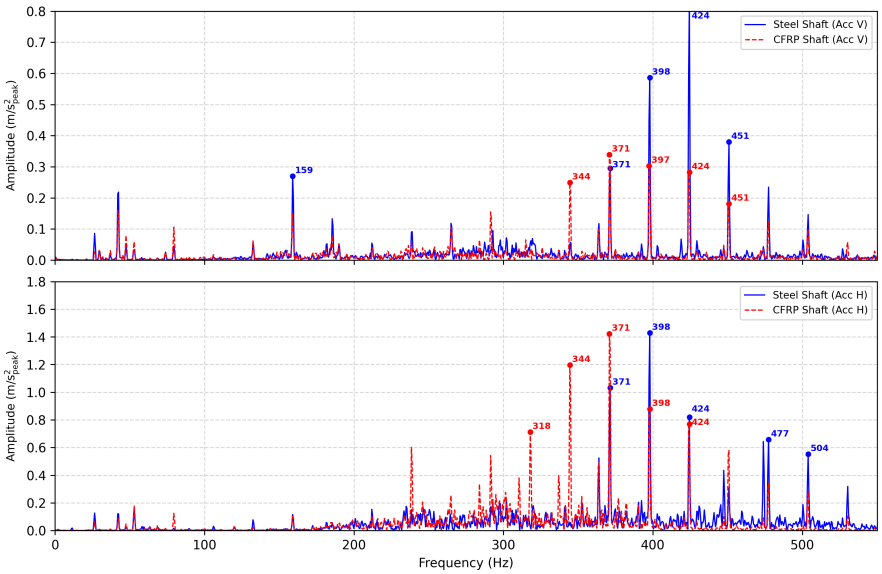


Fig. 10 FFT graph comparing Steel and CFRP shafts for $n = 1560$ rpm, $v_f = 117$ mm/min, $a_p = 0.5$ mm.

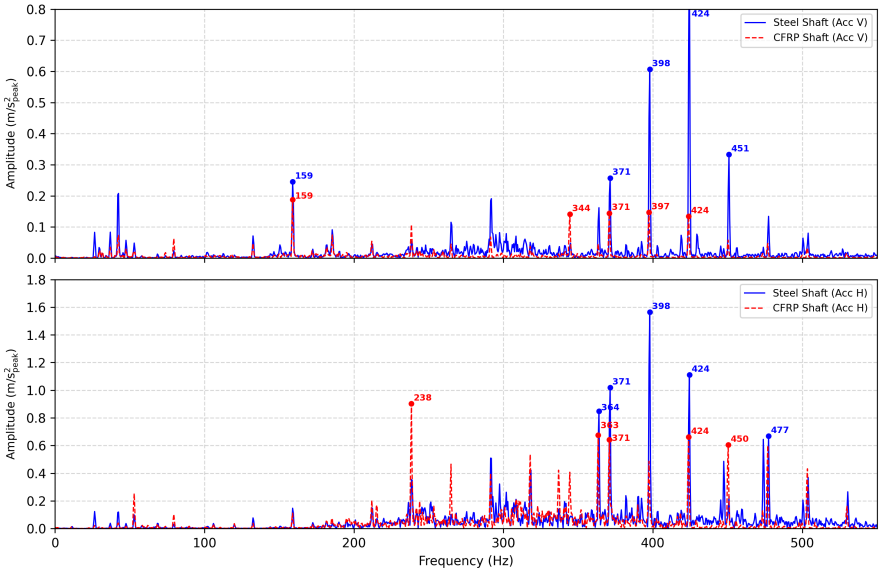


Fig. 11 FFT graph comparing Steel and CFRP shafts for $n = 1560$ rpm, $v_f = 117$ mm/min, $a_p = 1.0$ mm.

4 Conclusion

This study presented a pioneer experimental investigation into the rotordynamic behavior and workpiece surface finish achieved during horizontal peripheral milling using a custom hybrid CFRP composite spindle shaft compared to a conventional solid steel shaft. By correlating orthogonal orbital displacement trajectories, FFT frequency acceleration spectra, and surface profile metrics (R_a, R_z, and R_t), the physical role of intrinsic composite damping was comprehensively mapped. The main conclusions are summarized as follows:

1. **Structural and Damping Optimization:** The custom hybrid CFRP spindle shaft achieved a 55.5% reduction in total rotating mass (1.06 kg vs. 2.38 kg) while increasing the structural damping ratio by nearly two orders of magnitude (14.58% vs. 0.15%). The hybrid bonded joints provided reliable torque transmission without joint slippage or structural debonding under cyclic dynamic shock loading.
2. **High-Speed Damping Window:** Under high-speed dynamic cutting conditions ($n = 1560$ rpm), the hybrid CFRP shaft operated as an effective passive "structural filter." Viscoelastic matrix dissipation suppressed high-frequency resonant peaks within the 350–450 Hz band—most notably attenuating the severe 398 Hz and 424 Hz modes observed in the steel shaft. Under elevated material removal rates ($a_p = 1.0$ mm), this structural filtering yielded substantial enhancements in peak surface topography, reducing R_z by up to 27.5% and R_t by up to 34.2%.
3. **Micro-Cutting Compliance Boundary:** A critical operational limitation was identified at low feed-per-tooth regimes ($f_z = 2.67\,\mu$m/tooth, $a_p = 0.5$ mm), where undeformed chip thickness falls below the edge radius and the cutting mechanism shifts to elastic-plastic plowing and rubbing. Due to its reduced flexural modulus ($E_{\text{eff}} = 54.33$ GPa vs. 210 GPa for steel), the CFRP shaft experienced dynamic bending compliance under elevated radial thrust forces, triggering self-excited horizontal chatter (291 Hz, 344 Hz, 371 Hz) and severe surface degradation ($\Delta R_a = -130.2\%$).
4. **Orbit Dynamics vs. Surface Topology:** Although the lower mass of the CFRP shaft generated more pronounced high-frequency boundary ripples ("lobed" or "hairy" orbit morphology), it maintained a tighter macro-displacement center offset baseline ($R = 13.10$–14.42 mm vs. $R \approx 15.11$ mm for steel).
5. **Inertial vs. Viscoelastic Regimes:** In low-to-moderate speed regimes (456–810 rpm), the steel shaft consistently yielded superior surface quality. Under these conditions, high static flexural rigidity and rotating inertia are essential to resist quasi-static cutting forces, whereas viscoelastic matrix damping provides reduced benefits.

In conclusion, hybrid CFRP spindle shafts offer a highly viable, lightweight, and self-damped alternative for high-speed tangential milling, provided cutting parameters avoid the plowing-induced compliance boundary. Future research will focus on tailoring the fiber layup orientation angle and hybridizing ultra-high-modulus pitch-based carbon fibers with metallic cores to enhance static flexural rigidity (E_{eff}) without sacrificing passive internal damping capacity, as well as extending the experimental

validation to structural aluminum alloys (e.g., Al 7075-T6) and higher torque milling conditions.

Declaration of generative AI and AI-assisted technologies in the manuscript preparation process

During the preparation of this work, the authors used Google Gemini for grammatical proofreading, English language polishing, structural text organization, and minor formatting assistance. The authors reviewed and edited the output as needed and take full responsibility for the content of the published article.

References

Aggogeri F, Borboni A, Merlo A, et al (2017) Vibration damping analysis of lightweight structures in machine tools. Materials 10(3). https://doi.org/10.3390/ma10030297

Birk F, Ali F, Weigold M, et al (2020) Lightweight hybrid cfrp design for machine tools with focus on simple manufacturing. The International Journal of Advanced Manufacturing Technology 108:3915–3924. https://doi.org/10.1007/s00170-020-05535-z

Grechaniuk Y, Varodov K (2025) Influence of regenerative effect and mode coupling on the stability of milling operations. Machinery Energetics 16(3):58–69. https://doi.org/10.31548/machinery/3.2025.58

Kim J, Hegde H, young Kim H, et al (2022) Spindle vibration mitigation utilizing additively manufactured auxetic materials. Journal of Manufacturing Processes 73:633–641. https://doi.org/https://doi.org/10.1016/j.jmapro.2021.11.051

Kim S, Ahn SH (2024) A cfrp/steel hybrid rotating shaft for a high-speed motorized spindle. Journal of Manufacturing Processes 119:66–72. https://doi.org/https://doi.org/10.1016/j.jmapro.2024.03.072

Kondo R, Kono D, Matsubara A (2020) Evaluation of machine tool spindle using carbon fiber composite. International Journal of Automation Technology 14(2):294–303. https://doi.org/10.20965/ijat.2020.p0294

Li N, Wang H, Chi M, et al (2026) Design and dynamic characteristics analysis of carbon fiber-reinforced metal composite spindles with high length-to-diameter ratio. Metals 16(3)

Liu Y, Liu Z, Song Q, et al (2016) Development of constrained layer damping toolholder to improve chatter stability in end milling. International Journal of Mechanical Sciences 117:299–308. https://doi.org/https://doi.org/10.1016/j.ijmecsci.2016.09.003

Ma W, Yu J, Yang Y, et al (2021) Optimization and tuning of passive tuned mass damper embedded in milling tool for chatter mitigation. Journal of Manufacturing

and Materials Processing 5(1). https://doi.org/10.3390/jmmp5010002

Ozoegwu CG, Okokpujie IP (2021) Harmonic analyses of periodic milling forces and vibrations. IOP Conference Series: Materials Science and Engineering 1107:012017. https://doi.org/10.1088/1757-899X/1107/1/012017

Wan S, Li X, Su W, et al (2019) Active damping of milling chatter vibration via a novel spindle system with an integrated electromagnetic actuator. Precision Engineering 57:203–210. https://doi.org/https://doi.org/10.1016/j.precisioneng.2019.04.007

Yang Y, Dai W, Liu Q (2015) Design and implementation of two-degree-of-freedom tuned mass damper in milling vibration mitigation. Journal of Sound and Vibration 335:78–88. https://doi.org/https://doi.org/10.1016/j.jsv.2014.09.032

Zheng M, Chongyan C, Youkang Y, et al (2024) Vibration characteristics and machining performance of carbon fiber reinforced shaft in poor rigidity machining tool system. The International Journal of Advanced Manufacturing Technology 134:2637–2652. https://doi.org/https://doi.org/10.1007/s00170-024-14179-2

Statements and Declarations

The authors have no relevant financial or non-financial interests to disclose. All authors contributed to the study conception and design. Material preparation, data collection and analysis were performed by Everton Coelho de Medeiros. The first draft of the manuscript was written by Everton Coelho de Medeiros and all authors commented on previous versions of the manuscript. All authors read and approved the final manuscript.